# Point spread function analysis for GNSS-based multistatic SAR

Santi, Fabrizio; Antoniou, Michail; Pastina, Debora

*DOI:*
10.1109/LGRS.2014.2337054



*Document Version*
Publisher's PDF, also known as Version of record

*Citation for published version (Harvard):*
Santi, F, Antoniou, M & Pastina, D 2015, 'Point spread function analysis for GNSS-based multistatic SAR', *IEEE Geoscience and Remote Sensing Letters*, vol. 12, no. 2, 6871351, pp. 304-308.
https://doi.org/10.1109/LGRS.2014.2337054

# Point Spread Function Analysis for GNSS-Based Multistatic SAR

Fabrizio Santi, Michail Antoniou, and Debora Pastina

***Abstract*—This letter presents an analysis of the multistatic point-spread function (MPSF) for passive synthetic aperture radar (SAR) with navigation satellites as opportunity transmitters and a stationary receiver. It is shown that a noncoherent combination of bistatic SAR images, obtained by multiple, spatially separated satellites, can yield multistatic imagery that may be essentially improved in terms of resolution when compared with a single bistatic SAR image. The MPSF is derived analytically, for an arbitrary number of bistatic acquisitions and for any bistatic topologies. Analytical results are confirmed using both simulated and experimental data. The obtained result could be applied for the analysis of spatial resolution in multistatic real time radar, thus enabling the adaptive selection of the more suitable opportunity transmitters.**

***Index Terms*—Bi/multistatic synthetic aperture radar (SAR), generalized ambiguity function (GAF), global navigation satellite system (GNSS)-based SAR, point-spread function (PSF).**

## I. Introduction

OVER the last years, the bistatic synthetic aperture radars (BSARs) have been the focus of increasing research activity, [1]. A BSAR system uses spatially separated antennas for signal transmission and echo reception. Several bistatic configurations have been proposed, involving different combinations of transmitters and receivers either on moving platforms (spaceborne and airborne) [2]–[5] or stationary [6], [7]. The majority of such BSARs involve a radar system as the transmitter. Another possibility is to configure a passive system using satellite illuminators as transmitters of opportunity, and a receiver that could be moving or stationary on the ground. One such system uses global navigation satellite system (GNSS) as transmitters, such as Global Positioning System, GLObal NAvigation Satellite System (GLONASS), or the forthcoming Galileo and Beidou [8]. The feasibility of this system has been experimentally demonstrated for both moving and stationary receivers [9], [10]; however, this letter considers the stationary receiver case only.

The motivation for using GNSS as transmitters lies in the structure of the GNSS constellations. At any time of the day, there are 6–8 satellites in a single constellation (24–32 when all 4 GNSS systems are fully operational), illuminating any point on earth from different angles. All of these signals can be received and processed separately or jointly using a single receiver, essentially forming a multistatic passive radar system. This feature has a number of advantages. First of all, it provides the potential for persistent area monitoring anywhere in the world. In addition, images obtained from the same scene, but with different satellite illumination angles, may aid in terrain classification [11]. Furthermore, images obtained from different satellites may be fused to increase the amount of information in a given area.

The main drawback in using GNSS is that they were not designed for radar applications and therefore lack the power budget and resolution capabilities of dedicated SARs. Images with a suitable signal-to-noise ratio and azimuth resolution (3–4 m for the stationary receiver case) can be obtained by considering long dwell times on target (typically 4–5 min). However, the range resolution is defined by the GNSS ranging signal bandwidth. For example, the Galileo E5bQ signal has a bandwidth of approximately 10 MHz (perhaps the broadest bandwidth GNSS signal), offering a resolution of 15m in the quasi-monostatic case. Furthermore, range resolution degrades rapidly as the bistatic angle increases [8]. Therefore, until now, as a bistatic system, GNSS-based SAR was found appropriate only for applications where a coarse resolution is acceptable.

This letter considers the noncoherent combination of multiple BSAR images to provide multistatic imagery with improved resolution capabilities. Some initial considerations on this topic can be found in [12]. The idea is that different bistatic topologies yield point-spread functions (PSFs) with different orientations. Therefore, after their combination, a single multistatic PSF (MPSF) can be formed that is the intersection of all the individual PSFs. By appropriate selection of the bistatic topologies we may expect a dramatically improved resolution.

This letter is organized as follows: after recalling the bistatic PSF for BSAR in Section II, we define and analytically derive the MPSF in Section III; in Section IV, some simulated case studies are presented in order to show the potentialities of the system, and in Section V, the simulated analysis is confirmed by experimental data sets. Finally, some conclusions are drawn in Section VI.

## II. Bistatic PSF

We consider a ground-based stationary receiver collecting the signals emitted from a GNSS transmitter and reflected by a stationary scene. The 2-D bistatic resolution cell of such a system is fully described by the generalized ambiguity function (GAF) [14], [15]. In the hypothesis of narrowband signal and narrow synthetic aperture, it is given by the product of

Manuscript received January 17, 2014; May 21, 2014; accepted May 28, 2014. This work was supported by the Engineering and Physical Science Research Council under Project EP/G056838/1 of the U.K. Government.

F. Santi and D. Pastina are with the Dipartimento di Ingegneria dell'Informazione, Elettronica e Telecomunicazioni (DIET), University of Rome "La Sapienza," 00184 Rome, Italy (e-mail: santi@die.uniroma1.it).

M. Antoniou is with the School of Electronic, Electrical and Computer Engineering, University of Birmingham, Birmingham B15 2TT, U.K. (e-mail: m.antoniou@bham.ac.uk).

Color versions of one or more of the figures in this paper are available online at http://ieeexplore.ieee.org.

Digital Object Identifier 10.1109/LGRS.2014.2337054

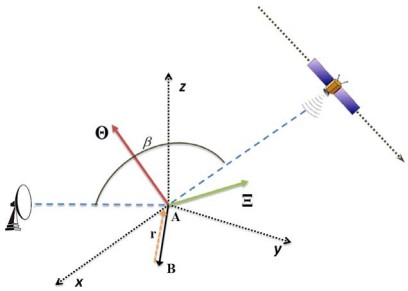


Fig. 1. BSAR geometry.

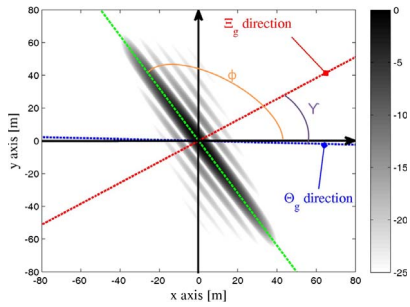


Fig. 2. Simulated bistatic PSF (intensity, log scale).

two normalized functions, $p(\cdot)$ and $m_A(\cdot)$. The former is the matched filter output of the ranging signal and the latter is the inverse transform of the normalized received signal magnitude pattern

$$|X(\boldsymbol{A},\boldsymbol{B})| \approx p\left(\frac{2\cos\left(\frac{\beta}{2}\right)\boldsymbol{\Theta}^T(\boldsymbol{r})}{c}\right)\cdot m_A\left(\frac{2_{\omega_E}\boldsymbol{\Xi}^T(\boldsymbol{r})}{\lambda}\right) \leq |X(\boldsymbol{A},\boldsymbol{A})| = 1 \quad (1)$$

where $\boldsymbol{A}$ is the vector position of the desired point reflector to be evaluated, vector $\boldsymbol{B}$ is an arbitrary position of another reflector in the vicinity of $\boldsymbol{A}$ and $\boldsymbol{r} = \boldsymbol{B} - \boldsymbol{A}$ (see Fig. 1); $\beta$ is the bistatic angle, and $\boldsymbol{\Theta}$ is a unit vector in the direction of its bisector; $\omega_E$ and $\boldsymbol{\Xi}$ are referred to as the equivalent angular speed and the equivalent motion direction (since a monostatic SAR moving in the direction $\boldsymbol{\Xi}$ with angular speed $\omega_E$ would exhibit similar Doppler-based resolution characteristics); and $c$ is the speed of light and $\lambda$ the wavelength.

In a BSAR the range resolution depends on the signal bandwidth B and the bistatic angle

$$\Delta R = \alpha_r \frac{c}{2B\cos\left(\frac{\beta}{2}\right)} \quad (2)$$

being $\alpha_r$ a factor accounting the shape of $p(\cdot)$; since the transmitted signal from a GNSS satellite is a pseudorandom code, the matched filter output can be approximated with a triangle function, and therefore, for the cut of $-3$ dB, $\alpha_r = 0.586$. Range resolution direction is specified by $\boldsymbol{\Theta}$. Azimuth resolution, which direction is specified by $\boldsymbol{\Xi}$, depends on the dwell time on target $T_d$ and the equivalent angular speed

$$\Delta A = \alpha_a \frac{\lambda}{2\omega_E T_d} \quad (3)$$

being $\alpha_a$ a factor accounting the shape of $m_A(\cdot)$; because of the long dwell times, the received signal magnitude pattern can be accurately modeled as a rectangular function and, as a consequence, $m_A(\cdot)$ is a *sinc* function and therefore, for the cut of $-3$ dB, $\alpha_a = 0.886$.

The projection of (1) onto the ground plane gives rise to a resolution cell that is approximately an ellipse (resolution ellipse), which can be evaluated using both numerical [12] and analytical methods. It is characterized by its orientation $\phi$, being function of the range and azimuth resolutions and of the angle $\gamma$ between their directions projected onto the ground plane, $\Theta_g$ and $\Xi_g$, respectively. Since in a bistatic system range and azimuth are generally not orthogonal, $\gamma$ differs from 90°. It should be also noted that according to their definition [8], the range and azimuth resolutions are indicators of a system's resolution capability, but their directions are not the ones where the spatial resolution is the worst. For example, Fig. 2 shows a simulated PSF for a scatterer in the scene center and a GLONASS satellite (having a bandwidth of 5.11 MHz); $\beta$ is about 71°, and $\omega_E$ is 0.005°/s; the dwell time is 200 s (therefore a linear trajectory of the satellite can be assumed [13]). The mutual positions of the receiver and the transmitter entail $\gamma \approx 34.2°$ and the orientation of the resulting resolution ellipse is $\phi \approx 122°$. The resolutions in the range and azimuth directions projected onto the ground plane, $\Delta R_g$ and $\Delta A_g$, respectively, are defined along $\Theta_g$ and $\Xi_g$. However, the worst spatial resolution, $\delta_{\max}$, is along the major axis (green line) of the PSF, whereas the best one, $\delta_{\min}$, is along the minor axis of the PSF, being very close to $\Xi_g$. Parameters $\delta_{\min}$ and $\delta_{\max}$ will be used to characterize the spatial resolution capability of this system hereafter, since they represent its lower and upper bounds [12]. In this example, the area of the resolution cell and the resolutions $\delta_{\max}$ and $\delta_{\min}$ (evaluated at the $-3$ dB contour hereafter) are about 163 $\mathrm{m}^2$, 44.5 m (whereas $\Delta R_g$ is 25.80 m) and 4.7 m (slightly better than $\Delta A_g = 5.12$ m), respectively.

## III. MPSF

### A. MPSF Using Noncoherent Addition

As previously stated, the use of GNSS transmitters makes possible long dwell times, on the order of 5 min or higher, allowing azimuth resolutions of 3-4 m, considerably greater than the range ones limited by the small signal bandwidth and, as follows from (2), by the bistatic angle. The coarse range resolution entails wide resolution cell areas, and this is made worse by the nonortoghonality between the azimuth and range resolution directions ($\gamma \neq 90°$). The most critical value is along the direction of the orientation of the resolution ellipse, $\phi$. In previous research [13], it was experimentally shown that using very long dwell times (10 min or more) provides some improvement in the resolution along $\phi$, as well as azimuth; however, the improvement factor was not sufficiently high.

In order to improve the resolution capability of the system, we derive a multistatic scheme formed by several bistatic couples, where the same receiver fixed on the ground collects the signals from different GNSS satellites, separates them by using frequency or coding division approaches, and combines all bistatic images obtained from them into a single, multistatic one. The idea is that different satellite positions and trajectories result in different bistatic PSF parameters: the $n$th bistatic PSF (1) is characterized by specific directions of range and azimuth resolutions and different values of the bistatic angle (2) and the equivalent angular speed (3). Different $\boldsymbol{\Theta}_n$ and $\boldsymbol{\Xi}_n$ result in a

TABLE I
SIMULATED ANALYSIS PARAMETERS

| Acquisition | Satellite (Cosmos) | $\beta$ [deg] | $\omega_E$ [deg/s] | $T_d$ [s] | $\Delta R_g$ [m] | $\Delta A_g$ [m] | $\delta_{max}$ [m] | $\delta_{min}$ [m] | $\gamma$ [deg] | $\phi$ [deg] | Area [m$^2$] |
|---|---|---|---|---|---|---|---|---|---|---|---|
| $A_1$ | 744 | 62.24 | 0.0045 | 300 | 22.74 | 3.98 | 67.23 | 3.62 | 19.46 | 79.91 | 189.21 |
| $A_2$ | 736 | 102.64 | 0.0048 | 250 | 43.09 | 4.14 | 49.10 | 3.85 | 59.33 | 37.64 | 144.37 |
| $A_3$ | 732 | 73.68 | 0.0048 | 200 | 26.74 | 4.97 | 26.88 | 4.83 | 80.64 | -9.54 | 93.91 |

different angle $\gamma_n$, whereas different $\beta_n$ and $\omega_{E_n}$ in different values of the range and azimuth resolutions $\Delta R_n$ and $\Delta A_n$. Finally, different $\gamma_n$, $\Delta R_n$, and $\Delta A_n$ result in different PSF orientations $\phi_n$. Therefore, a noncoherent combination of the individual PSFs, with their different orientations, results in a MPSF, whose resolution cell area is the overlapping segment of the single bistatic PSFs, and therefore may be essentially reduced. As a first step, the noncoherent addition method is considered, as it is a linear operation. We define as MPSF, the noncoherent addition of $N \geq 2$ PSFs

$$\text{MPSF}: \frac{1}{N}\sum_{n=1}^{N} p\left(\frac{2\cos\left(\frac{\beta_n}{2}\right)\boldsymbol{\Theta}_n^T(\boldsymbol{r})}{c}\right) \cdot m_A\left(\frac{2\omega_{E_n}\boldsymbol{\Xi}_n^T(\boldsymbol{r})}{\lambda}\right). \quad (4)$$

Similar combination strategies have been considered in the past for obtaining a multistatic radar system with improved performance; in [16] has been proved that different performance optimization criteria lead to different weightings of the several bistatic links. However, here we equally weight all the bistatic links, assuming a calibration step already performed so that all the bistatic channels can be considered affected by the same free space attenuation.

### B. Approximated Version of the MPSF

One of the features of the single-channel PSF represented by the GAF in (1) is that it is given by the product of two functions separately pertaining to the range and Doppler domain: even if the range and Doppler directions are not orthogonal their domains are still separable. For the MPSF in (4), this cannot be done since the summation and the modulus operator. However, it can be approximated as

$$\text{MPSF} \approx \bar{p}\bar{m} \quad (5)$$

being

$$\bar{p} = \frac{1}{N}\sum_{n=1}^{N} p_n = \frac{1}{N}\sum_{n=1}^{N} p\left(\frac{2\cos\left(\frac{\beta_n}{2}\right)\boldsymbol{\Theta}_n^T(\boldsymbol{r})}{c}\right) \quad (6)$$

$$\bar{m} = \frac{1}{N}\sum_{n=1}^{N} m_{A_n} = \frac{1}{N}\sum_{n=1}^{N} m_A\left(\frac{2\omega_{E_n}\boldsymbol{\Xi}_n^T(\boldsymbol{r})}{\lambda}\right). \quad (7)$$

In this expression, the range and Doppler domains are again separated. This approximation can be easily proven setting $p_n \approx p$, true in a wide zone around the mainlobe of the MPSF: since each $p_n(\cdot)$ function has a very wide mainlobe, due to the bistatic geometry, the limited bandwidth and the elevation angle of the satellite [8], the differences between the several $p_n(\cdot)$ can be assumed negligible, despite their different orientations.

## IV. SIMULATED RESULTS

Potentially, the noncoherent addition method can be applied to images obtained from different satellites, belonging to different navigation satellite constellations. However, in this analysis, satellites from the same GLONASS constellation are considered, being the constellation used for the experimental results verification [15]. Assume $N = 3$ bistatic geometries formed by GLONASS transmitters and a receiver fixed on the ground. The parameters of the simulation are reported in Table I along with the parameters of the resulting PSF, shown in Fig. 3. The worst resolution case has been found for Acquisition 1 $(A_1)$ that, despite the best ground range and azimuth resolutions (due to the smallest $\beta$ and longest $T_d$), has the minor angle $\gamma$, whereas the best one for $A_3$, where $\gamma \approx 90°$.

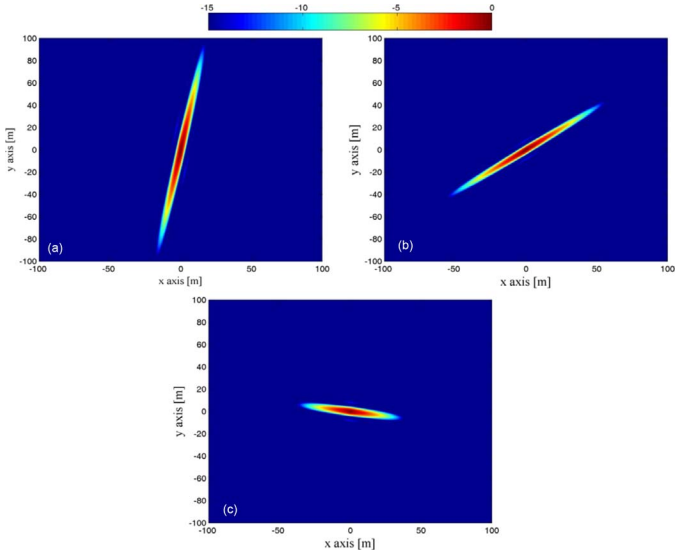


Fig. 3. Simulated bistatic PSFs (intensity, log scale). (a) $A_1$, (b) $A_2$, and (c) $A_3$.

In Fig. 4, we show the MPSF achievable by combining two bistatic channel [$A_1$ and $A_3$, Fig. 4(a)] and all the three bistatic PSFs [see Fig. 4(b)] using the same color scale as in Fig. 3. Comparing the bistatic PSFs in Fig. 3 and the MPSFs in Fig. 4, the reduction of the resolution cell area compared with the single PSFs is evident for $N = 2$. Increasing the number of combined channels, the main effect is the reduction of sidelobe levels around the peak, whereas the mainlobe region remains approximately the same as the one achieved by integrating two channels, as long as the transmitters positions entail different PSFs orientations. The cell sizes of the MPSFs are reported in Table II. Comparing the entries here to those of Table I, an improvement of the worst spatial resolution is achieved, and as a consequence a reduction of the resolution cell area of about five times can be seen between the bistatic and multistatic cases. Fig. 4(c) and (d) shows the approximated version of the MPSF achieved from (5) for the same cases in Fig. 4(a) $(A_1 + A_3)$ and Fig. 4(b) $(A_1 + A_2 + A_3)$. A good agreement between the nominal and the approximated version of the MPSF can be observed, particularly around the mainlobe. The error of the approximation can be calculated as the absolute difference between the real and approximated values of the MPSF, weighted pixel by pixel for the value. Fig. 5 shows

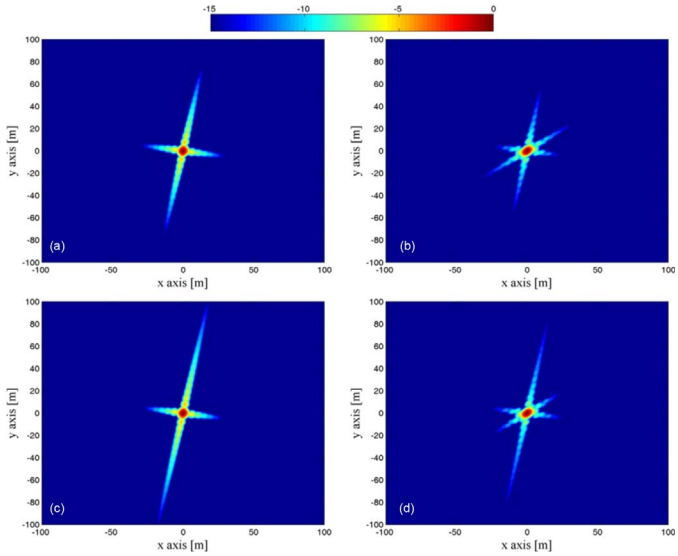


Fig. 4. Simulated MPSFs and their approximated version (intensity, log scale). (a) $A_1 + A_3$, (b) $A_1 + A_2 + A_3$, (c) $A_1 + A_3$ (approximated), and (d) $A_1 + A_2 + A_3$ (approximated).

TABLE II
SIMULATED MPSF RESOLUTION CELL AREA

| MPSF | $A_1$+$A_2$ | $A_1$+$A_3$ | $A_2$+$A_3$ | $A_1$+$A_2$+$A_3$ |
|---|---|---|---|---|
| $\delta_{max}$ [m] | 10.25 | 7.03 | 9.30 | 7.45 |
| $\delta_{min}$ [m] | 4.12 | 5.23 | 4.84 | 4.74 |
| Area [m$^2$] | 36.33 | 28.79 | 38.77 | 29.61 |

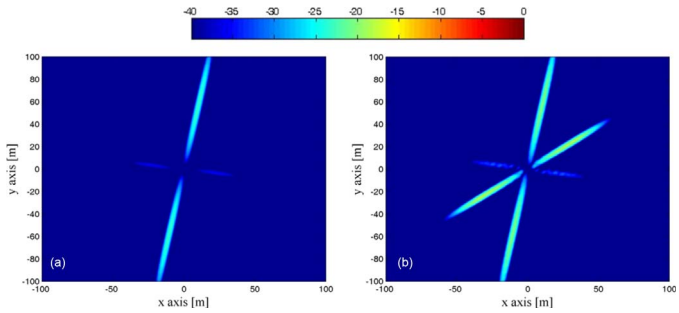


Fig. 5. Error of the MPSF approximation (intensity, log scale). (a) $A_1 + A_3$ and (b) $A_1 + A_2 + A_3$.

the errors for the approximated MPSF for the cases in Fig. 4, showing a negligible error in the mainlobe of the function and a limited error (below $-20$ dB) around it.

As in the bistatic case the minimum area is achieved when $\gamma \approx 90°$, in the multistatic case for $N = 2$ we expect the minimum value to be observed when $\Delta\phi = \phi_1 - \phi_2 \approx 90°$. For example, in the previous analysis, the smallest area for the multistatic case was found combining $A_1$ (with the poorest resolution) and $A_3$, since the two PSFs are nearly orthogonal. In order to show the resolution improvement as a function of the difference in PSF orientation, the following simulation scenario was carried out: a real GLONASS satellite trajectory 3-h long was considered, with satellite elevation angles greater than 45° throughout. In real situation, this would allow a low-gain antenna pointed toward the sky to record the GLONASS direct signal for the whole acquisition time without the need to steer it in the satellite's direction. The whole trajectory was then divided in $K$ frames, each one being $T_d$ s long. Each frame can yield a PSF whose orientation depends on the satellite position and direction during the frame interval. Therefore,

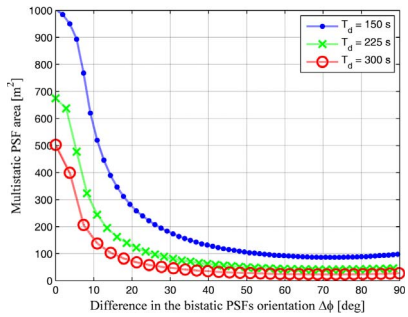


Fig. 6. MPSF area as a function of the difference in bistatic PSF orientation.

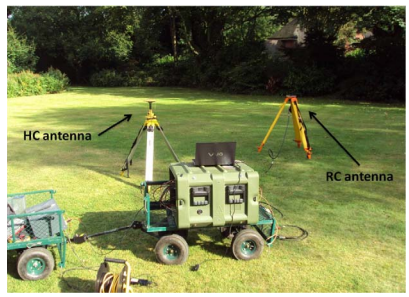


Fig. 7. Receiving hardware.

different frames have an angular separation $\Delta\phi$. Specifically the resulting PSF concerning frame 1 is combined following (4) with the PSFs from all the other frames, so $\Delta\phi = \phi_h - \phi_1$, $h = 1, \ldots, K$. Fig. 6 shows the area of the MPSF as a function of $\Delta\phi$. We can observe how for all the considered frame times the area greatly decreases with the increase of $\Delta\phi$, moving from values around 500–1000 m$^2$ for $\Delta\phi \approx 0°$ (where $\Delta\phi = 0°$ is the single PSF case) up to 50–100 m$^2$ when $\Delta\phi \approx 90°$.

## V. EXPERIMENTAL RESULTS

Data acquisitions using GLONASS satellites were conducted to confirm the proposed techniques. The experimental hardware, developed at the University of Birmingham, comprises a superheterodyne receiver with two channels. The first uses a low-gain antenna to collect the direct signal from the satellite, which is used for the synchronization providing the propagation delay and phase reference for image formation (heterodyne channel [HC]) [17]; the second uses a high-gain antenna receiving the signal reflections from the target area (radar channel [RC]). In this context, we are interested in experimentally obtaining the MPSF and compare it with theoretical results. Since in BSAR the use of passive point-like scatterers such as corner reflectors is not recommended, in order to emulate a point-like target both RC and HC antennas were pointed toward the satellite using low-gain antennas and we use the direct signals to generate the bistatic PSFs [13]. The experimental setup is shown in Fig. 7. The parameters of the acquisitions are reported in Table III; the experimental bistatic PSFs are shown in Fig. 8(a) and (c), along with the corresponding simulated ones [Fig. 8(b) and (d)], so that we can appreciate the very good accordance between simulated and experimental single-channel results. We observe that the two satellite trajectories result in two nearly orthogonal PSFs and therefore, according with the results in Fig. 6, we expect a considerably great improvement factor in the resolution cell area.

TABLE III
EXPERIMENTAL ANALYSIS—ACQUISITION AND BISTATIC PSFs PARAMETERS

| Acquisition | Satellite (Cosmos) | β [deg] | $\omega_E$ [deg/s] | $T_d$ [s] | $\Delta R_g$ [m] | $\Delta A_g$ [m] | γ [deg] | $\phi$ [deg] |
|---|---|---|---|---|---|---|---|---|
| A | 717 | 85.45 | 0.0049 | 300 | 31.28 | 3.25 | 62.78 | 43.77 |
| B | 716 | 100.14 | 0.0050 | 210 | 39.39 | 4.80 | 69.08 | 122.62 |

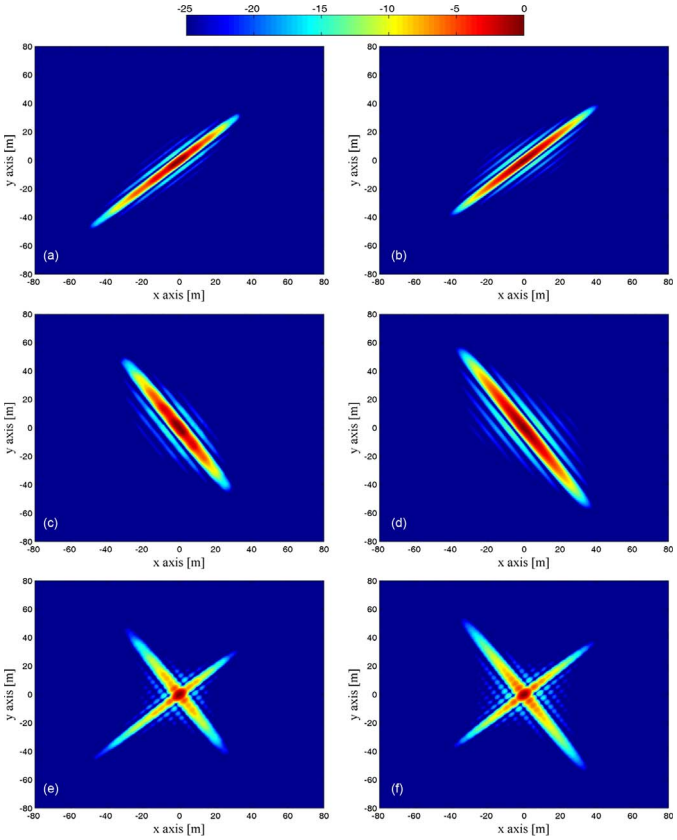


Fig. 8. Bi/MPSFs (intensity, log scale). (a) PSF A (experimental), (b) PSF A (simulated), (c) PSF B (experimental), (d) PSF B (simulated), (e) MPSF (experimental), and (f) MPSF (simulated).

TABLE IV
EXPERIMENTAL Bi/MPSF PARAMETERS

| | PSF A | PSF B | MPSF |
|---|---|---|---|
| $\delta_{max}$ [m] | 32.38 | 40.49 | 7.26 |
| $\delta_{min}$ [m] | 3.00 | 4.67 | 4.38 |
| Area [$m^2$] | 62.30 | 107.92 | 25.54 |

The resulting MPSF is shown in Fig. 8(e), with a good coincidence with the theoretical expectations [Fig. 8(f)]. In addition, Table IV reports the cell sizes of the Bi/MPSFs both for simulated and experimental results. It can be seen that the MPSF presents the worst spatial resolution that is improved of about four times with respect to worst resolution in the bistatic case, and the multistatic resolution cell area is approximately 2.5 and 4 times better than in data acquisitions A and B, respectively.

## VI. CONCLUSION AND FUTURE WORKS

This letter puts forward a multistatic SAR system using GNSS satellites as transmitters of opportunity and a receiver fixed on the ground. The use of such a technology is cost effective since only the development of the receiver is required and can be potentially used for persistent local area monitoring. The work here presented shows the theoretical analysis of the MPSF achieved combining the single images resulting from several GNSS satellites transmissions. Such a system has the potentiality to considerably improve the resolution cell with respect to the single bistatic channel case properly selecting satellites positions and trajectories. The theoretical analysis was verified by both simulations and experimental results. It is worth to notice that all the results are applicable for the configuration using a moving receiver, where a Doppler resolution less than 1 m is expected; therefore, in such a configuration, a resolution cell of about 1 $m^2$ could be achieved. The next step is to move from the point target analysis to the real images, in order to evaluate the full potential and challenges of the proposed technique.

## REFERENCES

[1] N. J. Willis, *Bistatic Radar*. Boston, MA, USA: Artech House, 1991.
[2] G. Krieger *et al.*, "TanDEM-X: A satellite formation for high-resolution SAR interferometry," *IEEE Trans. Geosci. Remote Sens.*, vol. 45, no. 11, pp. 3317–3341, Nov. 2007.
[3] I. Walterscheid, A. R. Brenner, and J. H. G. Ender, "Results on bistatic synthetic aperture radar," *Electron. Lett.*, vol. 40, no. 19, pp. 1224–1225, Sep. 2004.
[4] P. Dubois-Fernandez *et al.*, "ONERA-DLR bistatic SAR campaign: Planning, data acquisition, and first analysis of bistatic scattering behaviour of natural and urban targets," *Proc. Inst. Elect. Eng.—Radar Sonar Navigat.*, vol. 153, no. 3, pp. 214–223, Jun. 2006.
[5] M. Rodriguez-Cassola, S. V. Baumgartner, G. Krieger, and A. Moreira, "Bistatic TerraSAR-X/F-SAR spaceborne-airborne SAR experiment: Description, data processing and results," *IEEE Trans. Geosci. Remote Sens.*, vol. 48, no. 2, pp. 781–794, Feb. 2010.
[6] F. Balke, "Field test of bistatic forward-looking synthetic aperture radar," in *Proc. IEEE Radar Conf.*, May 2005, pp. 423–429.
[7] J. Sanz-Marcos, P. Lopez-Dekker, J. J. Mallorqui, A. Aguasca, and P. Prats, "SABRINA:A SAR bistatic receiver for interferometric applications," *IEEE Geosci. Remote Sens. Lett.*, vol. 4, no. 2, pp. 307–311, Apr. 2007.
[8] M. Cherniakov and T. Zeng, "Passive bistatic SAR with GNSS transmitters," in *Bistatic Radar: Emerging Technology*, M. Cherniakov, Ed. New York, NY, USA: Wiley, 2008.
[9] M. Antoniou and M. Cherniakov, "GNSS-based SAR: A signal processing view," *EURASIP J. Adv. Signal Process.*, vol. 2013, no. 1, pp. 98:1–98:16, May 2013.
[10] M. Antoniou, Z. Zeng, L. Feifeng, and M. Cherniakov, "Experimental demonstration of passive BSAR imaging using navigation satellites and a fixed receiver," *IEEE Geosci. Remote Sens. Lett.*, vol. 9, no. 3, pp. 477–481, May 2012.
[11] Z. Zeng, M. Antoniou, Q. Zhang, M. Hui, and M. Cherniakov, "Multi-perspective GNSS-based passive BSAR: Preliminary experimental results," in *Proc. 14th Int. Radar Symp.*, Jun. 2013, pp. 467–472.
[12] F. Daout, F. Schmitt, G. Ginolhac, and P. Fargette, "Multistatic and multiple frequency imaging resolution analysis—Application to GPS-based multistatic radar," *IEEE Trans. Aerosp. Electron. Syst.*, vol. 48, no. 4, pp. 3042–3057, Oct. 2012.
[13] F. Liu, M. Antoniou, Z. Zeng, and M. Cherniakov, "Point spread function analysis for BSAR with GNSS transmitters and long dwell times: Theory and experimental confirmation," *IEEE Geosci. Remote Sens. Lett.*, vol. 10, no. 4, pp. 781–785, Jul. 2013.
[14] T. Zeng, M. Cherniakov, and T. Long, "Generalized approach to resolution analysis in BSAR," *IEEE Trans. Aerosp. Electron. Syst.*, vol. 41, no. 2, pp. 461–474, Apr. 2005.
[15] M. Cherniakov and T. Zeng, "Space-surface bistatic SAR," in *Bistatic Radar: Emerging Technology*, M. Cherniakov, Ed. New York, NY, USA: Wiley, 2008.
[16] I. Bradaric, G. Capraro, D. D. Weiner, and M. C. Wicks, "Multistatic radar systems signal processing," in *Proc. IEEE Conf. Radar*, Apr. 2006, pp. 106–113.
[17] R. Saini, R. Zuo, and M. Cherniakov, "Problem of syncronisation in space-surfarce bistatic SAR based on GNSS emissions–Experimental results," *IET Radar, Sonar Navigat.*, vol. 4, no. 1, pp. 110–125, Feb. 2010.